Available online at www.sciencedirect.com

ScienceDirect

Mendeleev Commun., 2019, **29**, 710–712

Mendeleev Communications

Transport properties of iron-doped $BaZr_{0.9}Yb_{0.1}O_{3-\delta}$

Anna V. Kasyanova,[a,b] Anna O. Rudenko,[a] Natalya G. Molchanova,[a] Alexey I. Vylkov,[a,b] Julia G. Lyagaeva*[a,b] and Dmitry A. Medvedev*[a,b]

[a] *Institute of High Temperature Electrochemistry, Ural Branch of the Russian Academy of Sciences, 620137 Ekaterinburg, Russian Federation. E-mail: yulia.lyagaeva@ya.ru; dmitrymedv@mail.ru*

[b] *Ural Federal University, 620002 Ekaterinburg, Russian Federation*

DOI: 10.1016/j.mencom.2019.11.038

The iron doping improves the ionic and electronic components of the total conductivity of $BaZr_{0.9-x}Yb_{0.1}Fe_xO_{3-\delta}$, which can be considered as a mixed ionic-electronic conductor for membrane reactors and solid oxide fuel cells.

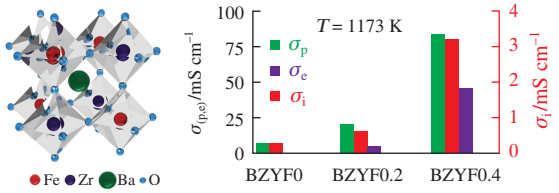

Mixed ionic-electronic conductors (MIECs) based on $BaZrO_3$ with a perovskite structure are of interest due to their promising electrical and catalytic properties. They can be used as electrochemical reactor membranes for partial oxidation of natural gas, functional electrode materials of solid oxide fuel cells (SOFCs), electrolysis cells (SOECs) and hydrogen sensors.[1–5] The $BaZrO_3$ ceramics doped with Y, Yb and Dy possesses a high bulk proton conductivity (10^{-2} cm^{-1} at 773 K) and good chemical stability in atmospheres containing water vapor and carbon dioxide.[6–8] To use these materials as membranes and SOFC electrodes, it is necessary to increase the electronic conductivity of $BaZrO_3$ by the insertion of transition elements (Fe or Co) in the B-sublattice of the ABO_3 perovskite structure.[9,10] The most promising dopant is iron due to its high solubility in the Zr-sublattice and good redox tolerance.[11–13]

Zhang with coauthors[14–16] studied the electrochemical properties of $BaZr_{0.9}Fe_{0.1}O_{3-\delta}$; however, they focused on the p-type conductivity and oxygen permeability. Kim with coauthors[11,12,17] reported the transport properties of iron-doped barium zirconate only in an atmosphere of air.

Here, we analyzed the transport properties of MIECs based on barium zirconate co-doped with iron and ytterbium.† Ytterbium is the most suitable acceptor dopant for $BaZrO_3$ in relation to transport properties.[18–20] The electrical conductivity of the materials was examined depending on oxygen partial pressure (p_{O_2}) to determine the contribution of electronic conductivity and the electrolyte domain boundary, which are important for optimizing the operating conditions of electrochemical devices.

According to XRD data, the sintered BZYFx ceramic samples have a cubic perovskite structure (space group $Pm\bar{3}m$); no extra reflections corresponding to impurity phases were found (Figure 1).‡ The unit cell parameters a of BZYF0, BZYF0.2 and BCZYF0.4 were 4.2249, 4.1863 and 4.1684 Å, respectively. The parameter a linearly decreases with iron content according to Vegard's rule. The change in a with Fe variation is attributed to the size factor since the ionic radius of iron (rFe$^{3+}_{HS}$ = 0.645 Å, rFe$^{3+}_{LS}$ = 0.550 Å) is lower than that of zirconium (rZr^{4+} = 0.72 Å).

Figure 2 shows the transport properties of the BZYFx samples.§ In the test temperature range, the materials have a semiconducting-type of conductivity, which increases with the iron concentration. For instance, these values reach 0.28, 1.02 and 2.88 mS cm^{-1} for BZYFe0 or 89.5, 106.4 and 128.9 mS cm^{-1} for BZYF0.4 at 873, 973 and 1073 K, respectively. The activation energy of conductivity of the BZYFx samples varies significantly, reflecting changes in electrotransfer nature.

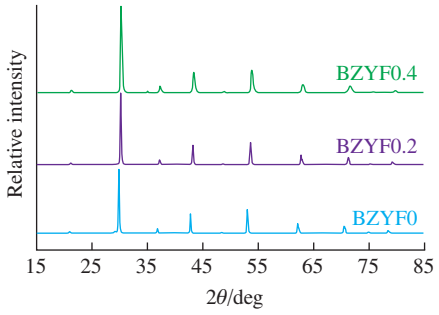

Figure 1 XRD patterns of the $BaZr_{0.9-x}Yb_{0.1}Fe_xO_{3-\delta}$ materials at room temperature.

† The complex oxides $BaZr_{0.9-x}Yb_{0.1}Fe_xO_{3-\delta}$ (BZYFx; x = 0, 0.2 and 0.4) were prepared using a citrate nitrate synthesis method. Nitrates of barium, ytterbium and iron and zirconium oxonitrate (purity, >99.5%) in stoichiometric amounts (taking into account crystallization water) were dissolved in distilled water at 423 K. Citric acid (in a molar ratio of 1 : 1 to the total amount of metal cations) was added under constant stirring. The resulting solution was accurately heated until complete water evaporation and residue auto-ignition. The highly disperse powders were annealed at 1073 K to remove carbon and organic residues; then, mechanical activation and preliminary synthesis were carried out at 1323 K (5 h). The ceramic samples were prepared by compacting the synthesized powders in the form of discs using a hydrostatic press followed by sintering the pressed materials at 1723 K for 5 h. The measured relative density of the ceramic samples was higher than 95%. The sintered samples were analyzed to confirm the formation of the specified compositions (Table S1, see Online Supplementary Materials) using chemical analysis (iCAP 6300 Duo inductively coupled plasma optic emission spectrometer).

‡ The ceramic materials were characterized by X-ray diffraction (XRD) analysis on a Rigaku D/MAX-2200VL/PC diffractometer. The scans were carried out at room temperature in the range $10° \leqslant 2\theta \leqslant 85°$ with a rate of 5 deg min^{-1} and a step of 0.02°.

§ The electrical conductivity of the samples was studied by a four-probe DC method in humid air in wide ranges of temperatures (T = 773–1173 K) and oxygen partial pressures ($10^{-20} \leqslant p_{O_2}$/atm $\leqslant 0.21$) at 1173 K using a Zirconia-318 device for the measurements of T and p_{O_2}.

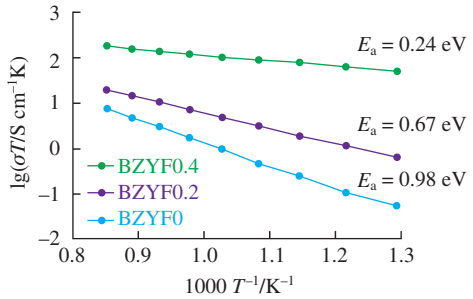

Figure 2 Total conductivity of the $BaZr_{0.9-x}Yb_{0.1}Fe_xO_{3-\delta}$ ceramic samples as a function of reciprocal temperature.

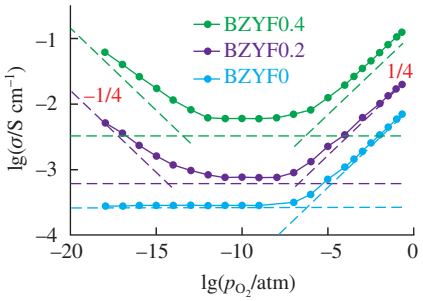

Figure 3 Total conductivity of the $BaZr_{0.9-x}Yb_{0.1}Fe_xO_{3-\delta}$ ceramic samples as a function of oxygen partial pressure at 1173 K.

Total conductivity was measured depending on p_{O_2} to investigate the effect of iron concentration on the transport properties of the BZYFx materials. Figure 3 shows three regions of $\lg\sigma = f(p_{O_2})$, in which a certain partial conductivity prevails. The first region corresponds to high p_{O_2}, where the total conductivity decreases when the p_{O_2} drops. The second is the medium p_{O_2} region; under these conditions, the conductivity attains almost constant levels. The last region corresponds to low p_{O_2}, where an increase in conductivity with a further p_{O_2} decrease for the BZYF0.2 and BZYF0.4 samples is observed, whereas the conductivity remains constant for the BZYF0 sample. To discuss the potential causes of different conductivity behaviors, possible defect formation and interactions between the oxides and gas atmospheres can be considered. To describe the quasi-chemical equations, the Kröger–Vink nomenclature was used.[21]

When doping barium zirconate with acceptors, such as Y_2O_3 and Fe_2O_3 (or FeO under certain p_{O_2} conditions), oxygen vacancies ($V_O^{\cdot\cdot}$) are generated according to the following equations:

$$Y_2O_3 \xrightarrow{BaZrO_3} 2Y'_{Zr} + V_O^{\cdot\cdot} + 3O_O^x, \quad (1)$$

$$Fe_2O_3 \xrightarrow{BaZrO_3} 2Fe'_{Zr} + V_O^{\cdot\cdot} + 3O_O^x, \quad (2)$$

$$2Fe'_{Zr} + O_O^x \xrightarrow{\text{low } pO_2} 2Fe''_{Zr} + V_O^{\cdot\cdot} + {}^1/_2O_2, \quad (3)$$

where Y'_{Zr} and Fe'_{Zr}, Fe''_{Zr} are acceptor defects located in the zirconium sublattice position, and O_O^x is the oxygen ion in its standard lattice position (Figure S1 confirms the partial reduction of Fe-ions ongradually decreasing p_{O_2}, Online Supplementary Materials).

At the high p_{O_2}, the dominant process is a reaction of gas oxygen with the oxygen vacancies resulting in the formation of new charge carriers, electron holes $h^{\cdot}$. The following equilibriums between the gaseous oxygen and oxygen vacancies in the solid phase can be written:

$${}^1/_2O_2 + V_O^{\cdot\cdot} \overset{K_p}{\longleftrightarrow} 2h^{\cdot} + O_O^x, \quad (4)$$

$$K_p = [O_O^x][h]^2(p_{O_2}^{1/2}[V_O^{\cdot\cdot}])^{-1} = p^2(p_{O_2}^{1/2}[V_O^{\cdot\cdot}])^{-1}, \quad (5)$$

$$p = K_p^{1/2}[V_O^{\cdot\cdot}]^{1/2}p_{O_2}^{1/4}, \quad (6)$$

where K_p is the equilibrium constant, and p is the concentration of electron holes. The p-type conductivity is directly proportional to the concentration of holes, giving the following power function of p_{O_2}: $\sigma_p \sim p_{O_2}^{1/4}$.

At low p_{O_2}, oxygen is released from the anion sublattice according to reaction (7). The equilibrium constant of this reaction (K_n) and the concentration of electron charge carriers (n) can be derived from the following equations:

$$O_O^x \overset{K_n}{\longleftrightarrow} {}^1/_2p_{O_2}^{1/2} + V_O^{\cdot\cdot} + 2e', \quad (7)$$

$$K_n = p_{O_2}^{1/2}[V_O^{\cdot\cdot}][e']^2[O_O^x] = p_{O_2}^{1/2}[V_O^{\cdot\cdot}]n^2, \quad (8)$$

$$n = K_n^{1/2}[V_O^{\cdot\cdot}]^{-1/2}p_{O_2}^{-1/4}. \quad (9)$$

The ratio of electronic conductivity and p_{O_2} can be simplified as follows: $\sigma_e \sim p_{O_2}^{-1/4}$.

At medium p_{O_2}, the conductivity remained almost unchanged with p_{O_2} variations due to the predominant ionic conductivity determined by the dopant concentration.

Thus, the total conductivity as a function of p_{O_2} can be described as a sum of three partial components:

$$\sigma_{total} = \sigma_i + \sigma_{e,o}p_{O_2}^{-1/4} + \sigma_{p,o}p_{O_2}^{1/4}, \quad (10)$$

where $\sigma_{p,o}$ and $\sigma_{e,o}$ are the p-type and n-type electronic conductivities, respectively, at p_{O_2} = 1 atm.

According to equation (10), the modeled dependences of the total and partial conductivities were processed and presented as dash-dotted lines in Figure 3. The Fe-doping of $BaZr_{0.9}Yb_{0.1}O_{3-\delta}$ increases both electronic and ionic total conductivity components; it is a key factor for using these materials as MIECs. In particular, the ionic conductivity at 1173 K increases from 0.28 mS cm^{-1} for BZYFe0 to 6.0 mS cm^{-1} for BZYFe0.4; the p-type electronic conductivity increases from 6.45 mS cm^{-1} for BZYFe0 to 83.6 mS cm^{-1} for BZYFe0.4, and the n-type electronic conductivity of BCZF0.4 is 45.85 mS cm^{-1} at p_{O_2} = 1×10^{-18} atm. Therefore, the observed decrease in activation energies (see Figure 2) is associated with electronic transfer caused by adding the transition iron ions rather than with dominant proton transportation, which is also characterized by lower values of E_a.

Thus, we examined the effect of iron concentration on the structural and transport properties of $BaZr_{0.9-x}Yb_{0.1}Fe_xO_{3-\delta}$. The single-phase ceramic samples were prepared using a citrate–nitrate synthesis. An increase in the iron content of the studied system leads to the improvement of both total and ionic conductivities. Therefore, the $BaZr_{0.4}Yb_{0.1}Fe_{0.4}O_{3-\delta}$ composition can be considered as a high-potential MIEC material for electrochemical applications.

This work was supported by the grant of the President of the Russian Federation for young scientists (grant no. MK-1654.2019.3).

Online Supplementary Materials

Supplementary data associated with this article can be found in the online version at doi: 10.1016/j.mencom.2019.11.038.

References

1 H. Dai, H. Kou, H. Wang and L. Bi, *Electrochem. Commun.*, 2018, **96**, 11.
2 Z. Tao, L. Yan, J. Qiao, B. Wang, L. Zhang and J. Zhang, *Prog. Mater. Sci.*, 2015, **74**, 1.
3 D. Medvedev, *Int. J. Hydrogen Energy*, 2019, **44**, 26711.
4 L. Bi, S. P. Shafi, E. H. Da'as and E. Traversa, *Small*, 2018, **14**, e1801231.
5 A. Volkov, E. Gorbova, A. Vylkov, D. Medvedev, A. Demin and P. Tsiakaras, *Sens. Actuators, B*, 2017, **244**, 1004.
6 K. D. Kreuer, *Annu. Rev. Mater. Res.*, 2003, **33**, 333.

7 D. Medvedev, J. Lyagaeva, S. Plaksin, A. Demin and P. Tsiakaras, *J. Power Sources*, 2015, **273**, 716.
8 Y. G. Lyagaeva, D. A. Medvedev, A. K. Demin, P. Tsiakaras and O. G. Reznitskikh, *Phys. Solid State*, 2015, **57**, 285 (*Fiz. Tverd. Tela*, 2015, **57**, 272).
9 Z. Wang, W. Yang, Z. Zhu, R. Peng, X. Wu, C. Xia and Y. Lu, *J. Mater. Chem. A*, 2014, **2**, 16707.
10 J. Zhang, Q. Yan, F. Wang, P. Yuan and P. Zhang, *J. Phys.: Condens. Matter*, 2000, **12**, 1981.
11 D. Y. Kim, S. Miyoshi, T. Tsuchiya and S. Yamaguchi, *ECS Trans.*, 2012, **45**, 161.
12 D. Kim, S. Miyoshi, T. Tsuchiya and S. Yamaguchi, *Solid State Ionics*, 2014, **262**, 875.
13 Y. Wu, K. Li, Y. Yang, W. Song, Z. Ma, H. Chen, X. Ou, L. Zhao, M. Khan and Y. Ling, *J. Alloys Compd.*, 2020, **814**, 152220.
14 H. Zhang and B. A. Wilhite, *Solid State Ionics*, 2016, **286**, 7.
15 H. Zhang, A. Suresh, C. B. Carter and B. A. Wilhite, *ECS Trans.*, 2014, **61**, 307.
16 H. Zhang and B. A. Wilhite, *J. Membr. Sci.*, 2016, **51**2, 104.
17 D. Kim, D. Lee and J. H. Joo, *J. Eur. Ceram. Soc.*, 2018, **38**, 535.
18 I. Ahmed, S.-G. Eriksson, E. Ahlberg, C. S. Knee, H. Götlind, L.-G. Johansson, M. Karlsson, A. Matic and L. Börjesson, *Solid State Ionics*, 2007, **178**, 515.
19 A. Satapathy and E. Sinha, *J. Alloys Compd.*, 2019, **772**, 675.
20 D. Han, N. Hatada and T. Uda, *J. Electrochem. Soc.*, 2016, **163**, F470.
21 F. A. Kröger and H. J. Vink, *Solid State Phys.*, 1956, **3**, 307.

Received: 6th May 2019; Com. 19/5911